Genes & Diseases (2020) 7, 138–149

Available online at www.sciencedirect.com

ScienceDirect

journal homepage: http://ees.elsevier.com/gendis/default.asp

FULL LENGTH ARTICLE

Three-dimensional printed tissue engineered bone for canine mandibular defects

Li Zhang [a,b], Junling Tang [c], Libo Sun [b], Ting Zheng [d], Xianzhi Pu [d], Yue Chen [e], Kai Yang [a,*]

[a] *Department of Oral and Maxillofacial Surgery, The First Affiliated Hospital of Chongqing Medical University, Chongqing 400016, China*
[b] *Department of Oral and Maxillofacial Surgery, Hospital of Stomatology Southwest Medical University, Luzhou, Sichuan, 646000, China*
[c] *Department of Hematology, The Affiliated Hospital of Southwest Medical University, Luzhou, Sichuan, 646000, China*
[d] *Department of Radiology, The Affiliated Hospital of Southwest Medical University, Luzhou, Sichuan, 646000, China*
[e] *Department of Nuclear Medicine, The Affiliated Hospital of Southwest Medical University, Luzhou, Sichuan, 646000, China*

Received 10 January 2019; received in revised form 1 April 2019; accepted 9 April 2019
Available online 8 May 2019

KEYWORDS
Mandibular defect;
Tissue engineering bone;
3D printing;
CAD/CAM;
BMSCs

Abstract *Background:* Three-dimensional (3D) printed tissue engineered bone was used to repair the bone tissue defects in the oral and maxillofacial (OMF) region of experimental dogs.
Material and methods: Canine bone marrow stromal cells (BMSCs) were obtained from 9 male Beagle dogs and in vitro cultured for osteogenic differentiation. The OMF region was scanned for 3D printed surgical guide plate and mold by ProJet1200 high-precision printer using implant materials followed sintering at 1250 °C. The tissue engineered bones was co-cultured with BASCs for 2 or 8 d. The cell scaffold composite was placed in the defects and fixed in 9 dogs in 3 groups. Postoperative CT and/or micro-CT scans were performed to observe the osteogenesis and material degradation.
Results: BMSCs were cultured with osteogenic differentiation in the second generation (P2). The nanoporous hydroxyapatite implant was made using the 3D printing mold with the white porous structure and the hard texture. BMSCs with osteogenic induction were densely covered with the surface of the material after co-culture and ECM was secreted to form calcium-like

* *Corresponding author.* Department of Oral and Maxillofacial Surgery, The First Affiliated Hospital of Chongqing Medical University, No. 1 Youyi Street, Yuzhong District, Chongqing, 400016, China.
E-mail addresses: alizdoctors@126.com (L. Zhang), ttjune@yeah.net (J. Tang), liboost@sina.com (L. Sun), tingtingair@sina.cn (T. Zheng), jr55597648@sina.com (X. Pu), asennianasen@163.com (Y. Chen), kai.kaiyang@yandex.com (K. Yang).
Peer review under responsibility of Chongqing Medical University.

https://doi.org/10.1016/j.gendis.2019.04.003

crystal nodules. The effect of the tissue engineered bone on the in vivo osteogenesis ability was no significant difference between 2 d and 8 d of the compositing time.
Conclusions: The tissue-engineered bone was constructed by 3D printing mold and high-temperature sintering to produce nanoporous hydroxyapatite scaffolds, which repair in situ bone defects in experimental dogs. The time of compositing for tissue engineered bone was reduced from 8 d to 2 d without the in vivo effect.

Introduction

The oral and maxillofacial (OMF) region is involved in the important physiological functions, such as breathing, chewing and speaking. The defects of the bone tissue in the OMF region are very harmful to the human body and usually caused by inflammation, trauma and tumors. The repair of the bone tissue defects is difficult because of the complicated anatomy of the OMF region with many organs, including the brain, eyes, vital teeth, nerves and blood vessel networks. The autologous bone transplantation is presently used to repair the defects of OMF bone tissue with some drawbacks, and often failed to meet the patient's requirements for appearance. The patients with the autologous bone transplantation may also suffer from the trauma from the surgery and/or postoperative dysfunctions.[1]

The cell-scaffold composite, or the tissue engineering, is the most ideal material for the repair of tissue and organ defects. The normal cells are in vitro cultured and amplified, and then inoculated on a biodegradable biomaterial scaffold to produce a cell scaffold-composite. The cells grown in the scaffold metabolize with nutrients, gas exchange and waste excreting. The tissue engineered prosthesis is implanted into the defects to replace the damaged tissues and organs for repairing and reconstructing the defects.[2] As a tissue regeneration technology, the tissue engineering effectively avoids trauma to the donor site and produces biomaterials to replace the autologous bone. The technique provides a new approach to repair the defects of the OMF bone tissue in clinical practices, and significantly reduces the patient's pain and overall cost. As a common method, bone marrow mesenchymal cells (BMSCs) are collected and in vitro amplified to induce osteogenesis, and then co-cultured with the constructed scaffold for 1—2 weeks, followed by the in vivo implantation. The procedure increases the waiting time for the implant surgery and the engineered bone with the constructed tissue is easily contaminated. The prolonged waiting time may also make some patients, such as patients with maxillofacial malignancies, missing the optimal timing for treatment.

The three-dimensional (3D) printing is the application of layer-by-layer printing technology to create 3D materials through computer-assisted design to achieve the rapid prototyping and build a complex of the organizational structure. As an emerging technology, 3D printing makes the highly matched scaffold based on the morphology of the defects.[3] Currently, the 3D printing technology is mainly applied in three aspects of the clinical practice, 1) construction of the solid model to guide clinical treatment, preoperative design and intraoperative guidance; 2) preparation of personalized prosthesis and implant for repairing defects and deformities, which is applied in clinical studies, such as 3D printed titanium alloy prosthesis for repairing mandibular defects; and 3) production of tissue engineered scaffold to repair and replace the original diseased tissue.[4—6] However, the current implant material, which is poorly biocompatible, would cause mechanical damage and chronic inflammatory reactions in adjacent tissues while it is existing in the body for a long time. The 3D printing to produce the tissue engineered bone scaffolds is now mainly in the laboratory stage. The number of patients who need to repair defects by using the tissue engineered bone is relatively small. The morphology of the scaffold materials by 3D printing is mostly individually customized but not mass-produced, which causes the high cost and the difficulty for the further research and clinical application.

In this study, based on the computer-assisted surgical technique, we have designed and resected the mandible part of the experimental dogs. By using 3D printing, we have produced the surgical resection guide plate and the mold of the defects. We have made the nanoporous hydroxyapatite scaffold by high-temperature sintering. After inducing and transforming into osteoblasts, the autologous BMSCs were inoculated into the nanoporous hydroxyapatite scaffold. The scaffold was implanted into the experimental dogs for the postoperative observation and analyses. Therefore, we have established a new method of the 3D printing technique to prepare the personalized scaffold with the convenience, accuracy and low cost. We hoped to provide more choices and reference indicators for the repair of bone tissue defects and the construction of tissue engineered bone in the oral cavity and maxillofacial region.

Methods

Ethical statement

All animal experiments were carried out in accordance with the US National Institute of Health (NIH) Guide for the Care and Use of Laboratory and approved by Institutional Animal Care and Use Committee (IACUC) and the ethics committee of the Animal Experimental Ethical Review of Southwest Medical University.

Isolation and in vitro culture of BMSCs

Canine bone marrow stromal cells (BMSCs) were obtained from 9 male Beagle dogs at the age of 11.5 ± 0.5 months. Under the general anesthesia, the bone marrow puncture was performed in the posterior superior iliac spine to collect 3 ml of the bone marrow fluid from each dog. Mononuclear cells (MC) were isolated from marrow using density gradient centrifugation.[7] Since BMSCs form adherent colonies in plastic culture vessels, after centrifugation, MC were collected from the sample/medium interface and plated in polystyrene culture plates containing Dulbecco's Modified Eagle Medium (DMEM) (GIBCO BRL, Grand Island, NY, U.S.A.) supplemented with 10% fetal bovine serum (FBS) (Nichirei Biosciences Inc., Tokyo, Japan, Batch #: 83300104), 100 IU/ml of penicillin and 0.1 mg/ml of streptomycin and incubated at 37 °C in 5% CO2 in a humidified chamber without disturbing the plates for 4 days. After removing nonadherent cells, adherent cells gently washed with PBS and cultured with the fresh media. Media were changed every 48 h until cells reached about 80–90% confluence. The primary (P0) monolayer colony forming unit cells were gently washed twice with PBS and detached using pre-warmed TrypLE™ Select CTSTM (GIBCO). Cells were passaged up to third passage (P3) in 100 mm culture plates at seeding density of 1×10^4 cells/cm^2 per subculture. At each passage (P0–P3), 1×10^6 cells were collected. The total RNA was extracted using TRIZol® Kit (Invitrogen, Life Technologies, Carlsbad, CA, U.S.A.) according to the manufacturer's instructions to evaluate expression of chondrogenic phenotype genes. Cell viability and total cell density was determined using 0.5% Trypan blue stain and manual hemocytometer cell counting method. The cell morphology and proliferation characterization were determined using a light microscope. BMSCs were finally obtained from adherent cultures of untreated whole bone marrow, in a white cloud-like layered interface. Most of the nucleated cells were located at this layer, and $1–2.5 \times 10^7$ cells/ml of nucleated cells were obtained in 3 ml of bone marrow fluid.

Osteogenic differentiation of BMSCs and Alizarin red staining

Cell osteogenic differentiation was inducted in the second generation (P2) of BMSCs in the experimental group. BMSCs were cultured in the osteogenic differentiation medium (ODM) containing 100 nM dexamethasone, 10 mM β-glycerophosphate and 50 μM ascorbic acid (Sigma–Aldrich, St. Louis, MO, USA). The media were changed every 3 days for 15 days. The P2 of BMSCs without osteogenic induction were used as the control group. For Alizarin red staining, BMSCs cells on the slide were washed with PBS, and then stained with Alizarin red for 30 min. After washing with the steamed water for 5 s 3 times, the slide was dried at room temperature, and then mounted with 80% glycerol-PBS for observation.

Preoperative design and production of scaffold

A 64-row and 128-slice spiral CT machine was used for plain scan of OMF region of the Beagle dog, with a layer thickness of 0.63 mm. The data was output in DICOM 3.0 format. The CT data was imported into the Geomagic Foundation 2013 software to generate a digital 3D image, which was converted into a stereolithography (STL) format file, and then transferred to the MIMICS software for the surgery design of animal mandibular bone defects. The bone tissue was resected with 18 mm long, 9 mm wide and 5 mm high of the bilateral mandibular body. The surgical guide plate was designed by the software according to the resection of range and the mold of making implant. The ProJet1200 high-precision printer was used to rapidly produce the surgical guide plate and molds, which were made from implant materials. The nanoporous hydroxyapatite implant material was made by the printing mold with the high temperature sintering. The nano-hydroxyapatite powder was mixed with polyethyleneimine to form a gel, and then fully stirred with polyoxyethylene and lauryl ether. The multifunctional epoxy compound and water-soluble cross-linking agent were added. The materials were poured into the mold made by 3D printing after the mixture became solidified. The mold was taken out after molding, and then placed in a vacuum atmosphere furnace at 1250 °C for sintering.[8]

Characterization of scaffold materials

Pore size and porosity

The prepared nanoporous hydroxyapatite implant materials were taken and placed in a material container, which was placed in a scanning chamber parallel to the Micro-CT rotating shaft. The parameters of the scanning were set as follows: scanning layer thickness 25 μm, current 140 μA, voltage 70 kV.

The content of saturated liquid

The sterile water was dropped on the nanoporous hydroxyapatite scaffold material for 5 μl each time until saturation. The content of saturated liquid was detected.

Morphological detection

Electron microscopy scanning: The nanoporous hydroxyapatite scaffold was placed in a 2.5% glutaraldehyde phosphate buffer, and then fixed in a refrigerator at 4 °C for 24 h. After washing with PBS, the nanoporous hydroxyapatite scaffold was placed in stages of 70%, 80%, 90%, 100% ethanol for 30 min each, and then in isoamyl acetate for 30 min. After drying at room temperature, the nanoporous hydroxyapatite scaffold was plated with the gold film for observation.

Production of tissue engineered bone

Grouping and culture

The tissue engineered bones in the TEB8D (control) group were in vitro co-cultured for 8 days, and in the TEB2D (experimental) group for 2 days. The P2 BMSCs with osteogenic induction were centrifuged at 1000 rpm for 3 min, resuspended with the OriCell™ canine bone marrow mesenchymal stem cell osteogenic differentiation medium, and then formulated into a 2×10^7/ml cell suspension. The nanoporous hydroxyapatite implant material was

transferred into a 6-well plate for use. The materials were divided into two planes: the convex (A) and flat (B) planes. Each plane was instilled with a cell suspension of about 160 μm. The gently repeated suck action during the instillation resulted that the cell suspension was evenly inhaled by the material. Five milliliters of OriCell™ canine bone marrow mesenchymal stem cell complete medium was added for incubation in a 37 °C, 5% CO_2 incubator for 6 h. The medium was removed and OriCellTM canine bone marrow mesenchymal stem cells osteogenic differentiation medium was added.

Observation on growth of the in vitro cultured tissue engineered bone

The cell-scaffold composite specimens were divided into 4 parts in the equal proportions along the long axis 2 d and 8 d after the co-culture, respectively, and marked as 1) the outer layer and 2) middle-outer layer of TEB8D (control) group, 3) outer layer and 4) middle-outer layer of middle layer TEB2D (experimental) group. The electron microscopy was used for observation.

Laboratory animal grouping and implantation surgery

Nine Beagle mandibles were randomly divided into three groups (n = 3/group) according to the implantation procedure. Group 1 (blank control) was implanted with nano-hydroxyapatite blank scaffold; Group 2 (experimental control) was the TEB8D scaffold composite group; Group 3 (experiment) was the TEB2D scaffold composite.

After the animal was anesthetized, an incision was made along the lower edge of the mandible. The skin, subcutaneous, muscular layer and periosteum layer were incised. The tissue flap was fully turned up to expose the surgical area with a periosteal stripper. The surgical guide plate was placed at a predetermined position of the mandible. The part of the mandibular bone substance was completely removed by the dynamic system according to the positioning of the surgical guide plate and the preoperative design. The cell scaffold composite was placed in the defects after excision and firmly fixed with titanium plates and titanium nails. After hemostasis, the wound was washed with saline, and the suture were completed. The wound was covered with the dress that was removed 2 d later. The animals were placed in cages and fed with enough food and water.

Postoperative CT and micro-CT scans

The CT scans were performed 3 and 6 months after the surgery and the micro-CT scans 9 months after the surgery on the jaw bones of the dog to observe the osteogenesis and material degradation. The healing of the mandibular bone defects was evaluated by plain scan and reconstruction of the three-dimensional data. Five planes were selected in the tissue engineered bone for measurement of the CT value on the implanted scaffold. The CT values were presented as the average of 5 measurements of the scaffold material on the side of defects (Hounsfield Unit, HU).

Gross observation of sample collection by postoperative electron microscopy

The titanium plate and titanium nail were removed by the dynamic system 9 months after the surgery. The bone tissue was resected about 5 mm around the implant to observe the healing of the implant and surrounding bone tissues. After removal, the surface of the implant was carefully washed with saline and fixed with 4% paraformaldehyde. The specimen was Micro-CT scan with Postoperative electron microscopy cut along the long axis centerline. The morphology of the implant material surface and material center was observed under electron microscope.

Postoperative hard tissue slicing and methylene blue-acid fuchsin staining

The specimen was fixed in a formaldehyde for 48 h, and then rinsed with ultrapure water for 24 h. After gradient dehydration with 60%, 80%, 90% and 100% alcohol, respectively, the specimens were placed in the resin embedding solution for impregnation for 10 d, and then in a vacuum bonding tableting device for fixing and bonding. The sections were prepared using the E300CP type microtome machine, and then stained with methylene blue-acid fuchsin following drying, transparentizing, and sealing. The histology of the section was observed.

Statistical Analysis

An ANOVA test was applied to define a difference among treatment groups, which was followed by a post-hoc multiple comparisons test to define specific group differences. Values of $p < 0.05$ were considered significant and $p < 0.01$ very significant.

Results

Morphology and osteogenic induction of BMSCs

Seventy-two hours after starting the primary culture, BMSCs were observed under an inverted microscope. The sporadic adherent cells were scattered between suspended cells, which had a short-fusiform, triangle or polygon shape with strong light refraction from the cytoplasm (Fig. 1A). Eleven days after the culture, the primary cells spread across the bottom of the culture plate. As the cell density increased, the cells changed from polygonal to spindle-shaped and gradually merged into a long-fusiform shape and grew in aggregates (Fig. 1B). According to the results of cell counting, the number of BMSCs in P1 generation was $5.1 \pm 2.3 \times 10^6$/mL and rapidly increased to $15 \pm 1.9 \times 10^6$/mL in P2 generation. By Alizarin red staining, no any nodular formation nor calcium deposits was observed in BMSCs without osteogenic induction, indicating no mineralized area formation (Fig. 1C), but many purple-red nodules in BMSCs with osteogenic induction, indicating the calcium formation (Fig. 1D). The data confirm that BMSCs with osteogenic induction were differentiated into osteoblasts.

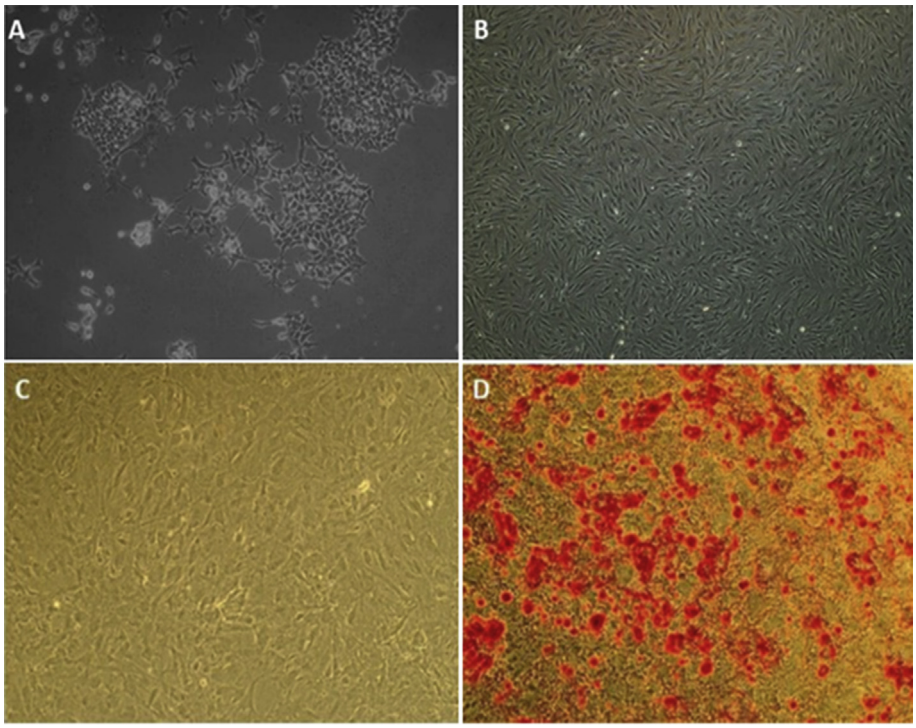

Figure 1 Morphology of and Alizarin red staining of BMSCs. Morphology of BMSCs after 3 days (**A**) and 11 days (**B**) (×40). Morphology of BMSCs after osteogenic differentiation (×40 in A and ×100 in B) and Alizarin red staining in BMSCs without (**C**) or with (**D**) osteogenic induction (×40).

3D printing and characterization of the scaffold

Micro-CT was used to scan the maxillofacial bone of the experimental dogs. The three-dimensional (3D) model of the maxillofacial bone was generated based on the CT data (Fig. 2A). The mandibular osteotomy was performed by removing the part of canine mandibular bone and applying the MIMICS software after data transfer (Figs. 2B, 1 and 2). According to the range of mandibular bones based on our designed resection, the surgical guide plate was designed for the canine modeling surgery (Fig. 2B, 3 and 4). In accordance with the shape of resected mandible, the implant material mold was designed for the production of scaffold (Fig. 2B, 5 and 6). The ProJet 1200 high-precision printer was used to rapidly produce the surgical guide plate (Fig. 2B, 7) and molds for implant scaffold (Figs. 2B, 8—9). The nanoporous hydroxyapatite implant was made by a high temperature sintering using the 3D printing mold (Figs. 2B, 10—12).

The characterization of 3D printing scaffold materials was detected including the pore size, the porosity, the content of saturated liquid and morphological features. The diameter of scaffold material pore ranged from 100 to 600 μm and the porosity of scaffold material ranged from 30 to 70%. Micro-CT scanning of nano-porous hydroxyapatite scaffold was showed in Fig. 3A—C. The content of saturated liquid of the nanoporous hydroxyapatite material was 320 μl/block. The nanoporous hydroxyapatite had the white porous structure with the hard texture and easy forming. The scanning electron microscopy (SEM) showed that the material had a large pore size, a great quantity of pores and relatively good connectivity between pores (Fig. 3D—F).

Morphology of tissue engineered bones in different groups

In the extracellular matrix (ECM) in the TEB 8D (control) group, a large number of cells with many deposits, including calcium salt crystals and collagen fiber-like substances, were observed in the outer layer. The perfect condition and many pseudopods indicated BMSCs with osteogenic induction on the material grew well (Fig. 4A). In the TEB 2D (experimental) group, there were a relatively large number of cells and many ECM deposits, including calcium salt crystals and collagen fibrin. Most cells protruded the pseudopods and connected with surrounding cells and materials (Fig. 4B). In the middle-outer layer, there was a large number of cells and many deposits, including calcium salt crystals and collagen fiber-like substances in the surface of the material in the TEB 8D (control) group. The cell morphology was full, and the cells were connected with the pseudopods (Fig. 4C). In the TEB 2D (experimental) group, there was a relatively large number of cells with full cell morphology and a small number of cells with protruded pseudopods and ECM deposits (Fig. 4D). In the inner layer, there was a relatively small number of cells with polygonal shape and complete cellular structure. The ECM deposits, including calcium salt crystals and collagen fiber-like substances, begun to occur. The pseudopods were protruded from the cells and collagen fibrin-like substances were observed (Fig. 4E). In the TEB 2D (experimental) group, there was an extremely small number of cells and ECM. The pseudopods of the cells were short and small (Fig. 4F).

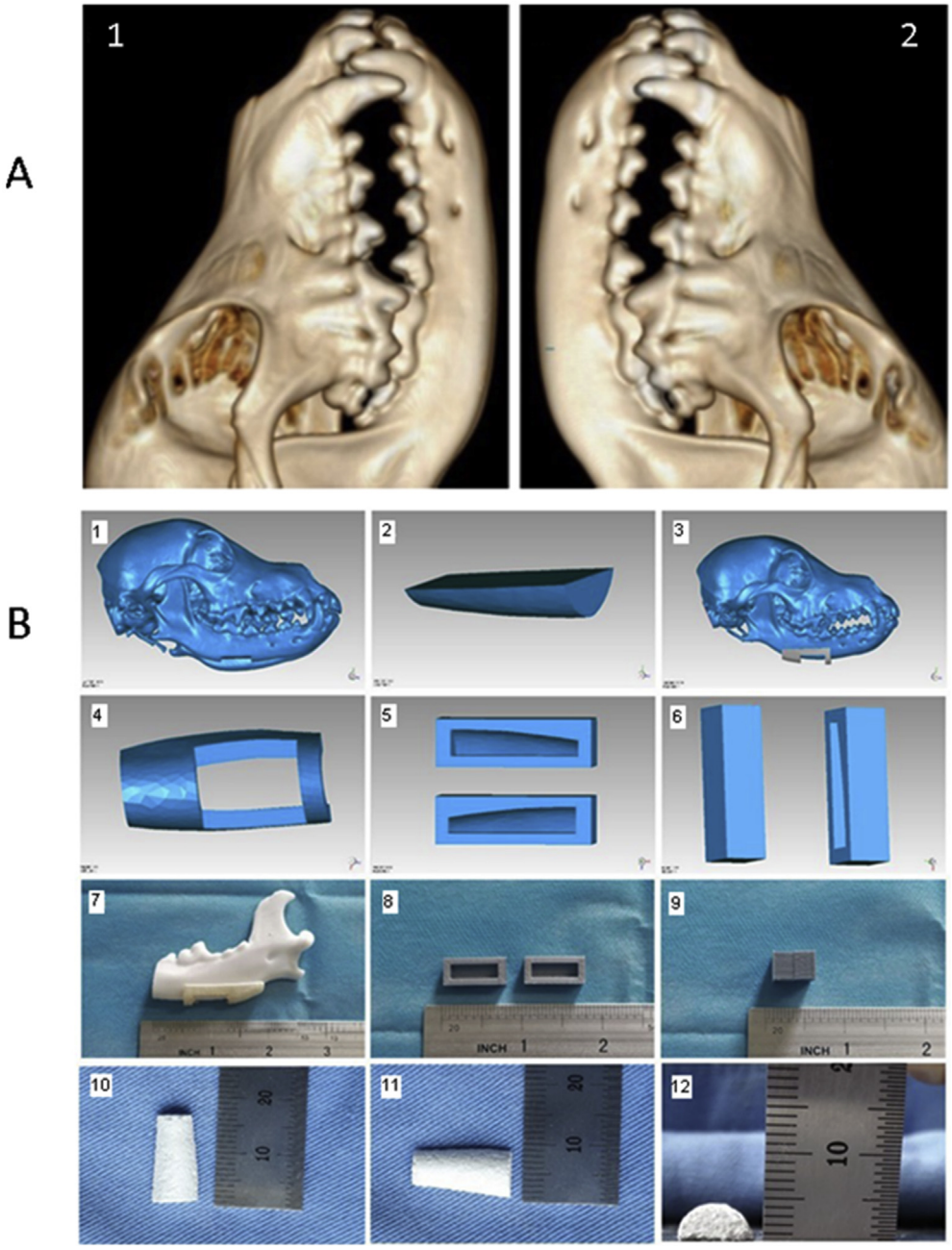

Figure 2 The maxillofacial bone micro-CT 3D images and the implant material mold for mandibular osteotomy. (**A**) Micro-CT 3D reconstruction images of right side (1) and left side (2) of the maxillofacial bone. (**B**) The design and production of implant material mold for mandibular osteotomy. (1, 2) mandibular osteotomy; (3, 4) the surgical guide plate according to resected scope; (5, 6) the implant material mold; surgical guide plate (7) and implant scaffold (8, 9); the (10) length, (11) width and (12) height of 3D printing implant scaffold.

BMSCs with osteogenic induction were densely covered with the surface of the material after co-culture and ECM was secreted to form calcium-like crystal nodules. Collagen fiber-like substances were observed in the TEB 8D and the TEB 2D groups, indicating that nanoporous hydroxyapatite scaffold materials had the good biocompatibility to BMSCs with osteogenic induction, which could promote the growth, proliferation and osteogenesis of BMSCs with osteogenic induction. After co-culture, the cells grew well, without a large number of cell death. There was no significant difference between the TEB 8D and the TEB 2D groups in the cellular morphology in the outer layer of the scaffold. The cell growth of the middle-outer layer in the TEB 2D group was slightly worse than that in the TEB 8D group, without significant differences in the cell number and cellular status. In the inner part of the materials, the number of BMSCs with osteogenic induction in the TEB 8D group was larger than that in the TEB 2D group. The growth state of BMSCs in the TEB 8D group was also better than that in the TEB 2D group. The results indicate that the

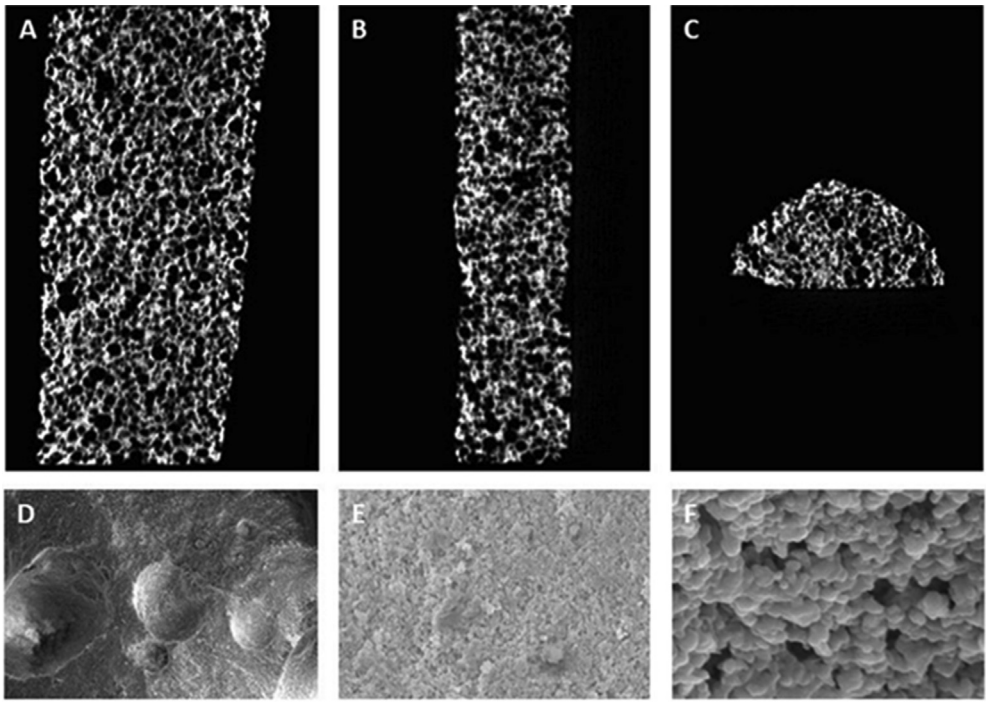

Figure 3 Micro-CT scanning of nano-porous hydroxyapatite scaffold. Micro-CT scan images: (**A**) Frontal film; (**B**) lateral film; (**C**) axial film. of Micro-CT scan images and SEM images of nano-porous hydroxyapatite scaffold in the magnification of (**D**) ×100, (**E**) ×500, and ×1000 (**F**) ×1000.

shortening of in vitro co-culture time has little effect on the growth of cells in the outside of the scaffold due to the poor nutrition in the inner part of the scaffold, resulting in poor cell growth and proliferation rate of the inner part in the TEB2D group.

Postoperative CT and Micro-CT scanning

The surgical procedure of the jaws of Beagle dogs included place the surgical guide plate on the predetermined position of the mandible (Fig. 5A), remove the designed mandibular bone using surgical guide plate (Fig. 5B), place the tissue engineered bone in the defect site (Fig. 5C), and fix the tissue engineered bone fixed with titanium plate and nail (Fig. 5D). The CT scans of jaws were performed 3 and 6 months postoperatively.

In the group 1, CT scans showed that no evidence of implants healed with bone substance at 3 and 6 months postoperatively, and the gap d with the surrounding bone was filled with low-density soft tissue (Fig. 5A, row a). In the group 2, the tissue engineered bone implants were gradually healed with the mandible and the surrounding bone (Fig. 6A, row b). In the group 3, the scaffold formed a bone connection with the periphery of the mandible and healed well with the surrounding bone (Fig. 6A, row c).

Nine months after surgery, micro-CT scans showed that the material was degraded without obvious formation of new bone in the pure nanoporous hydroxyapatite in the group 1 (Fig. 6B, row a). In the groups 2 (Fig. 6B, row b) and 3 (Fig. 6B, E a), the tissue engineered bones were healed well with the surrounding bones and the trabecule-like structures. The implants formed bone connected with the defect edge of the mandible.

According to the measurement, the CT value of group 1 was decreased from 1181.6 ± 5.89 HU at 3 months to 1080.99 ± 26.3 HU at 6 months, and declined to 906.48 ± 11.16 HU at 9 months; the CT value of group 2 was increased from 1218.19 ± 21.45 HU at 3 months to 1654.41 ± 22.66 HU at 6 months, and finally reached 1809.56 ± 15.57 HU at 9 months; the CT value of group 3 was increased from 1214.92 ± 8.46 HU at 3 months to 1616.63 ± 19.6 HU at 6 months, and finally increased to 1786.53 ± 14.68 HU at 9 months. There were no significant differences of CT values within three groups at 3 months postoperatively ($P > 0.05$). However, the CT values of the group 2 and 3 were slightly higher than that of the group 1, indicating that new bone had begun to appear in the implant materials in the group 2 and 3, but no bone tissue formation in the scaffolds in group 1. Six and nine months after surgery, the mean CT values of group 2 and 3 were higher than that of group 1 ($p < 0.01$) (Fig. 6C). The nanoporous hydroxyapatite scaffold would gradually degrade in vivo, and the bone mineral density of the tissue engineered bone was maintained at a level close to the normal bone density. However, the simple scaffold group had no obvious new bone formation with the prolongation of time, but the implant materials were gradually degraded, resulting that the density was gradually decreased. At 3, 6 and 9 months after surgery, there were no differences in CT values between the group 2 and 3 ($p > 0.05$). Both groups were healed well at 9 months after surgery, indicating that the two groups had similar osteogenesis ability (Fig. 6C).

Nine months after surgery, the boundary between the implants and the two broken ends were still clear and the

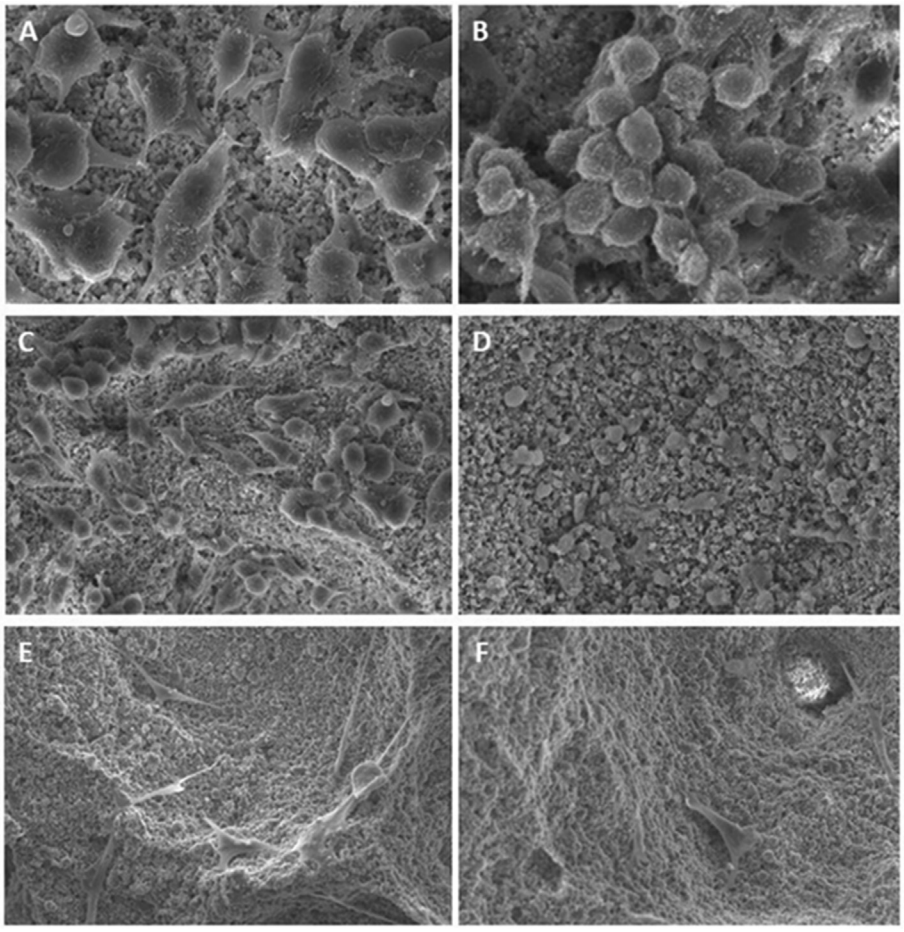

Figure 4 SEM images of the outer (**A**—**B**), middle-outer (**C**—**D**) and inner (**E**—**F**) surface from nano-porous hydroxyapatite scaffolds treated with BMSCs in the TEB 8D group (**A, C, E**) and TEB 2D group (**B, D, F**).

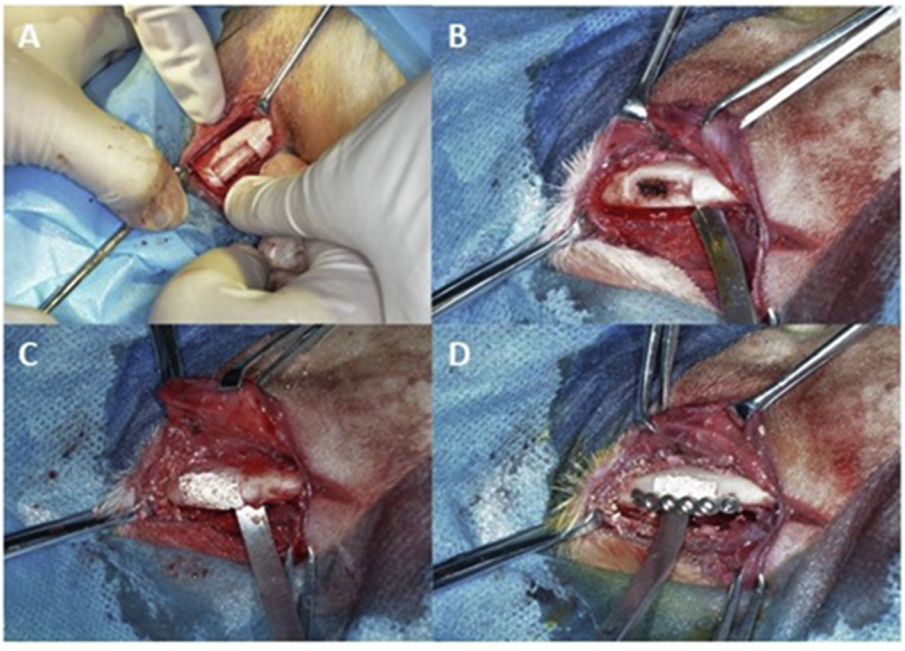

Figure 5 The surgical procedure of the jaws of Beagle dogs. (**A**) The surgical guide plate was placed on the predetermined position of the mandible; (**B**) the designed mandibular bone was completely removed by using surgical guide plate; (**C**) the tissue engineered bone was placed in the defect site; (**D**) the tissue engineered bone was firmly fixed with titanium plate and nail.

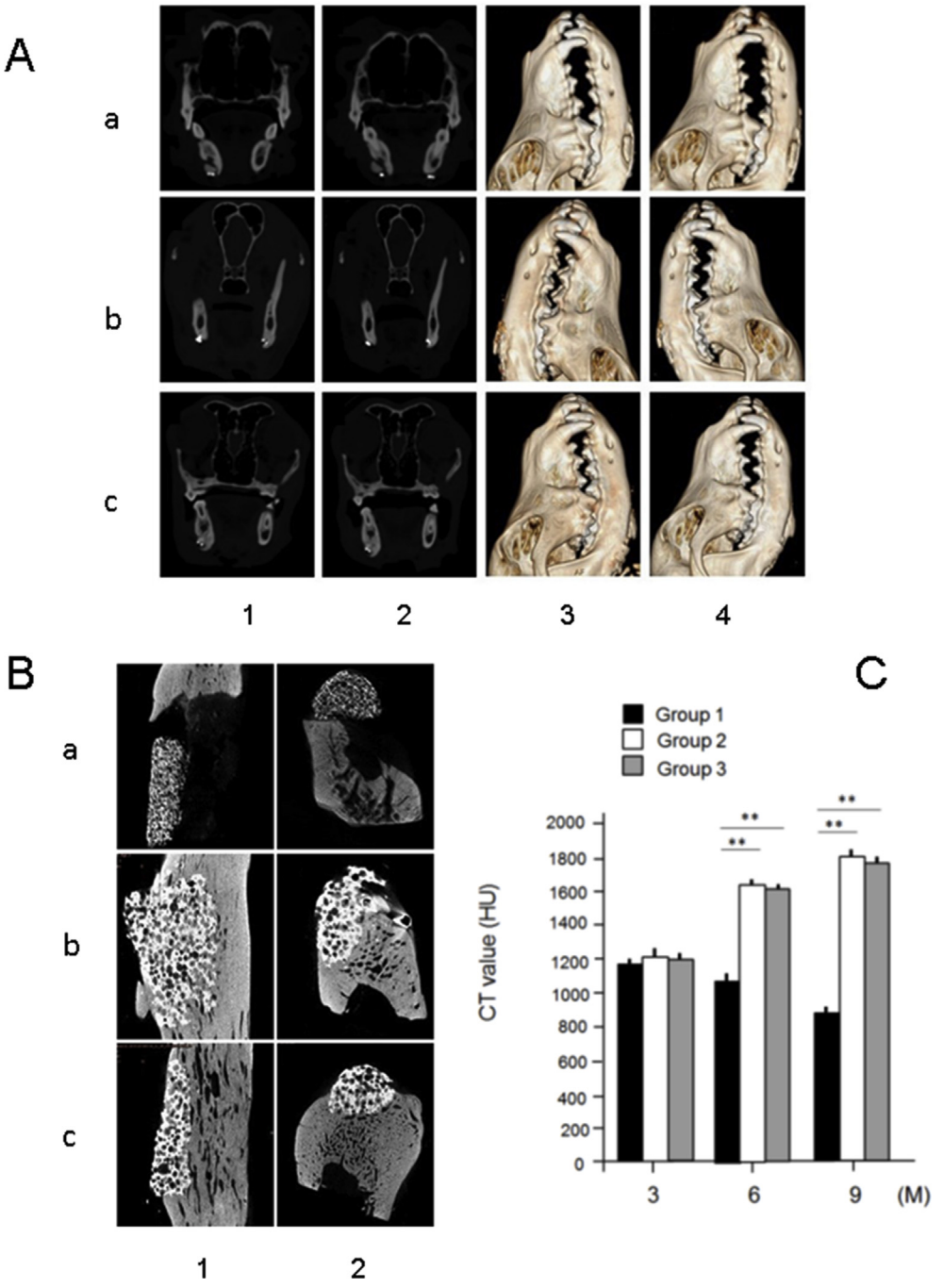

Figure 6 3D images and comparison of CT values of the jaws of Beagle dogs after surgery. (**A**) The CT scans (line 1-2) and 3D reconstruction images (line 3-4) of Beagles' jaws 3 (line 1, 3) and 6 months (line 2, 4) after the surgery in postoperatively. As forthe group 1 (row a), the group 2 (row b) and the group 3 (row c). (**B**) 3 and 6 months postoperatively of CT scans (A-B) and 3D reconstruction images (**C**). **(ns: $p > 0.05$; ***$p < 0.0001$).

soft tissue was filled in the middle in the group 1. There was no obvious osteotylus on the surface nor inflammatory reaction in the surrounding tissues (Fig. 7A, B). In the groups 2 and 3, the tissue engineered bones were well healed without inflammatory reaction in surrounding tissues, indicating that the tissue engineered bone repairs mandibular defects in vivo and maintains mandibular integrity due to its good histocompatibility (Fig. 7C—F). However, simple nanoporous hydroxyapatite scaffolds in the group 1 could not repair the mandibular defects.

Postoperative morphology of implant scaffold

Nine months after surgery, a small amount of fusiform, polygonal cells and ECM deposits were observed on the

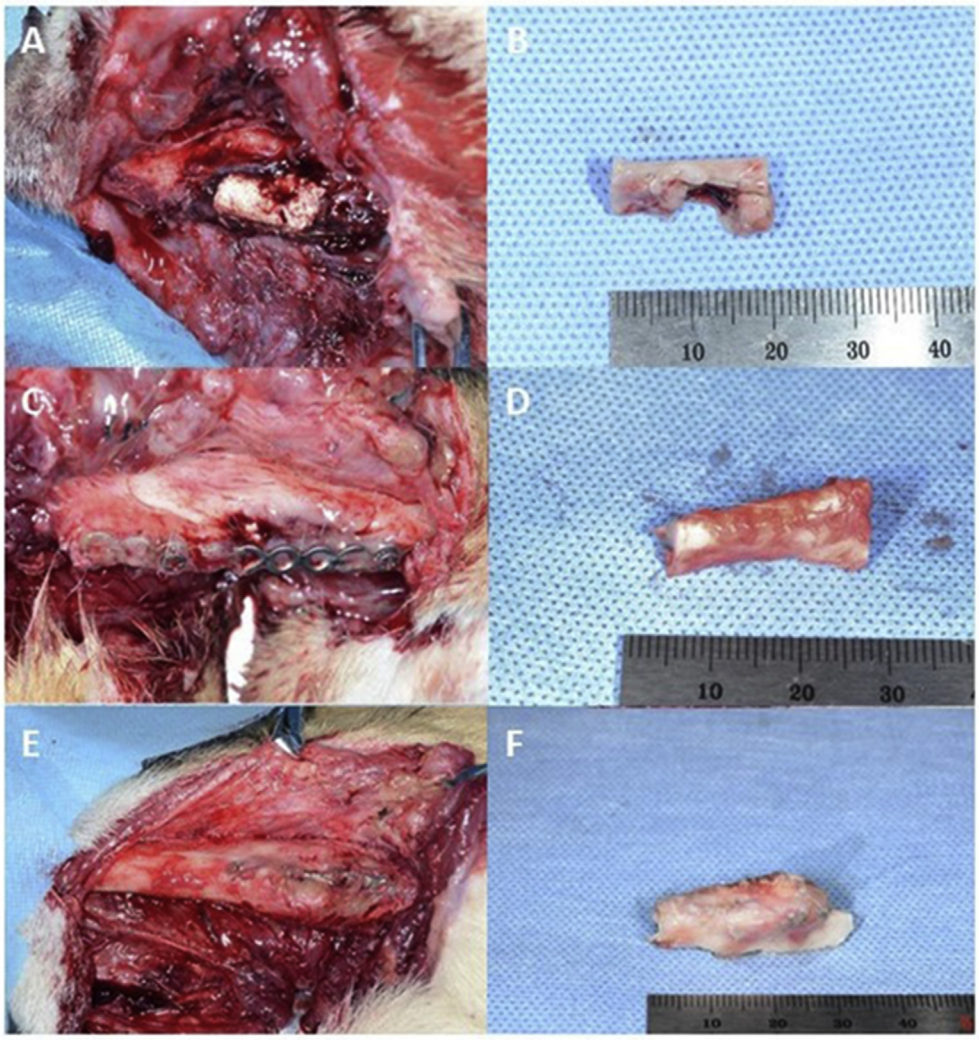

Figure 7 Gross observation of tissue engineered bones in the group 1 (**A**—**B**), 2 (**C**—**D**) and 3 (**E**—**F**).

surface of material internal pore without obvious phenomenon of material osteogenesis in the group 1 (Fig. 8A, B). Haversian canals and dense ECM deposits were occurred in the internal part of implants in the groups 2 and 3 (Fig. 8D, E). We also observed mineral crystals and well-arranged collagen fibers around the Haversian canals (Fig. 8G, H). Fig. 8 showed the methylene blue-acid fuchsin staining of bone tissues. In the group 1, the formation of the bone tissue was rare with a small number of osteocytes and degraded scaffolds (Fig. 8C). The internal part of tissue-engineered bones in the group 2 (Figs. 8F) and 3 (Fig. 8I) were relatively apparent and structurally similar to Haversian canals. The osteocytes were arranged in an order manner and bone connections were formed between the edge of the bone defect and the normal bone.

Discussion

The materials for the scaffolds of the tissue engineered bone include bioceramics, bone cement and new composite scaffolds.[9] No any single material fully meets all conditions for the construction of ideal tissue engineered bone. Hydroxyapatite with a certain physical strength is widely used to repair small bone defects in the clinical practice,[10] because its internal microstructure is similar to the bone tissue. However, the application of hydroxyapatite in repairing bone defects is limited due to some problems, such as the uneven degradation rate in the body, excessive hardness and poor flexibility.[11] In the recent years, researchers have been trying to introduce the nanotechnology into the production of porous hydroxyapatite.[12] By studying the biological activity, the degradation properties, biocompatibility, osteoconductivity and structural strength of the nanoporous hydroxyapatite has been greatly improved for repairing the large isolated bone defects.[13,14]

The principle of 3D printing technology is to use computer to assist the design and then export the data to a printer. The adaptive material is precisely and quickly molded by layer-by-layer stacking.[15] The 3D printing technology is divided into the fused deposition modeling (FDM), stereolithography appearance (SLA), selective laser singeing (SLS), digital light processing (DLP), laminated object manufacturing (LOM) and 3D bioprinting.[15]

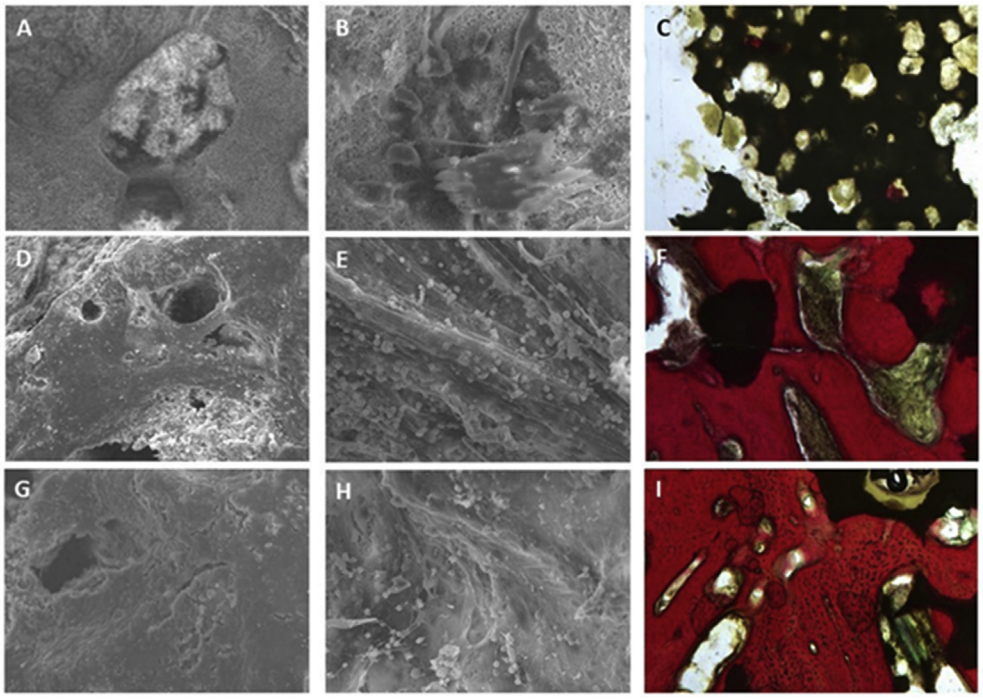

Figure 8 SEM images of implant scaffold and methylene blue/acid fuchsin staining of bone tissues in the three groups after surgery. (**A**) ×100, (**B**) ×300 and (**C**) section staining in the group 1; (**D**) ×100, (**E**) ×300 and (**F**) section staining in the group 2; (**G**) ×100, (**H**) ×300 and (**I**) section staining in the group 3.

In this experiment, we have used SLA to make a surgical guide plate, which matches the shape of the canine mandible, for the precise removal of the parts and scaffold mold in the experimental dogs. The photosensitive material in SLA is rapidly molded under ultraviolet light with the fine molding precision (about 100 μm), the high quality of the surface and the low cost of the materials.[15]

The printed mold is prepared by a high-temperature sintering method to produce a nanoporous hydroxyapatite scaffold, which is highly consistent with the morphology of canine mandibular bone defects with 100—600 μm of the average pore diameter, 30—70% of the porosity, the pores connected to each other to form the network-like spatial structures. The scaffold is similar to the normal cancelous bone and meets the needs for constructing the tissue engineered bone. The high-temperature sintering method has widely been used in industrial manufacturing and precision machining with the decrease in the cost and manufacturing cycle. Combined with SLA printing, the high-temperature sintering method achieves 100 μm of the high processing precision, which fully meets the clinical requirements for repair of bone defects.

We have in vitro induced and expanded BMSCs to reach the standard requirement of the number of cells for the construction of the tissue engineered bones, and then to composite and culture with the scaffold material. The traditional co-culture time is about 1—2 weeks, and the total time for making engineered bones is often one month. The long co-culture time increases the possibility of failure of the constructed tissue engineered bones. In this experiment, contamination occurred during co-culture composition, resulting a delay of the implantation surgery for about 1 month. We have cultured cells outside the cell-scaffold composites for 8 days in the TEB8D (control) group and 2 days in the TEB2D (experimental) group, to investigate whether the waiting time before the transplantation could be shortened. The electron microscopy observation indicates that the shortening in vitro co-culture time affect the growth of the cells in the scaffold. By using CT and micro-CT at the different time-points, we have observed that the mandibular defects were well repaired in two groups.

In the present study, we have found that BMSCs are suitable as the seed cells for tissue engineered bone. BMSCs with osteogenic induction are indispensable in the process of repairing bone defects. Consistent with many reports, the nanoporous hydroxyapatite scaffold produced by high-temperature sintering method composited with BMSCs are capable to repair a large range of bone defects in the maxillofacial region. We have also found that shortening the composite time of BMSCs with osteogenic induction and porous hydroxyapatite scaffolds has no effect on the ability of tissue engineered bone to repair bone defects.

Our experimental results demonstrate the importance of the seed cells and the microenvironment in the formation of tissue engineered bone. As the seed cells, BMSCs differentiate into osteoblasts, and secrete cytokines that participates in the immunoregulation of osteogenesis. For relatively small bone defects, simple bioceramic materials guide the relevant cells around the defects to repair by crawling. However, the cell crawling could not repaire the relatively large bone defects. The osteogenic differentiation and immunomodulatory capacity of BMSCs are indispensable in repairing bone defects. We have also confirmed that a simple nanoporous hydroxyapatite scaffold could not be osteogenesis. Therefore, BMSCs are necessary for repair

of the large bone defects. For tissue defect repair, the microenvironment is always an important factor in initiating tissue regeneration, especially for the application of stem cells as a treatment. By comparing the in vitro growth of tissue engineered bone cells and the final formation of tissue engineered bone in the environment of the bone defect area, we have found that the microenvironment in the mandibular bone defect promotes the cell growth in the center of the material.

In conclusion, we have constructed the tissue-engineered bone by 3D printing mold and high-temperature sintering to produce nanoporous hydroxyapatite scaffolds, which in situ repair bone defects in experimental dogs. We have also reduced the time of compositing for tissue engineered bone from 8 d to 2 d without the effect on the in vivo osteogenesis ability of the tissue engineered bone.

Ethics approval and consent to participate

The study was approved by the Animal Experimental Enthical Review From Of Southwest Medical University. Informed consent was obtained.

Conflict of interest

The authors declare no conflict of interest.

Acknowledgments

This study is supported by the This study was supported by the Scientific Research Project of Sichuan Education Department Project (14ZA0141).

Appendix A. Supplementary data

Supplementary data to this article can be found online at https://doi.org/10.1016/j.gendis.2019.04.003.

References

1. Kuroda S, Katayama A, Takano-Yamamoto T. Severe anterior open-bite case treated using titanium screw anchorage. *Angle Orthod*. 2004;74:558—567.
2. Credi C, Biella S, De Marco C, Levi M, Suriano R, Turri S. Fine tuning and measurement of mechanical properties of cross-linked hyaluronic acid hydrogels as biomimetic scaffold coating in regenerative medicine. *J Mech Behav Biomed Mater*. 2014; 29:309—316.
3. O'Brien CM, Holmes B, Faucett S, Zhang LG. Three-dimensional printing of nanomaterial scaffolds for complex tissue regeneration. *Tissue Eng Part B Rev*. 2015;21:103—114.
4. Cvetkovic C, Raman R, Chan V, et al. Three-dimensionally printed biological machines powered by skeletal muscle. *Proc Natl Acad Sci U S A*. 2014;111:10125—10130.
5. Michael S, Sorg H, Peck CT, et al. Tissue engineered skin substitutes created by laser-assisted bioprinting form skin-like structures in the dorsal skin fold chamber in mice. *PLoS One*. 2013;8:e57741.
6. Espitalier F, Vinatier C, Lerouxel E, et al. A comparison between bone reconstruction following the use of mesenchymal stem cells and total bone marrow in association with calcium phosphate scaffold in irradiated bone. *Biomaterials*. 2009;30: 763—769.
7. Pittenger MF. Mesenchymal stem cells from adult bone marrow. *Methods Mol Biol*. 2008;449:27—44.
8. Kneser U, Stangenberg L, Ohnolz J, et al. Evaluation of processed bovine cancellous bone matrix seeded with syngenic osteoblasts in a critical size calvarial defect rat model. *J Cell Mol Med*. 2006;10:695—707.
9. Canter HI, Vargel I, Mavili ME. Reconstruction of mandibular defects using autografts combined with demineralized bone matrix and cancellous allograft. *J Craniofac Surg*. 2007;18: 95—100. discussion 1-3.
10. Liu G, Sun J, Li Y, et al. Evaluation of partially demineralized osteoporotic cancellous bone matrix combined with human bone marrow stromal cells for tissue engineering: an in vitro and in vivo study. *Calcif Tissue Int*. 2008;83:176—185.
11. Isaksson H, Tolvanen V, Finnila MA, et al. Long-term voluntary exercise of male mice induces more beneficial effects on cancellous and cortical bone than on the collagenous matrix. *Exp Gerontol*. 2009;44:708—717.
12. Loken S, Jakobsen RB, Aroen A, et al. Bone marrow mesenchymal stem cells in a hyaluronan scaffold for treatment of an osteochondral defect in a rabbit model. *Knee Surg Sports Traumatol Arthrosc*. 2008;16:896—903.
13. Zioupos P, Cook R, Coats AM. Bone quality issues an matrix properties in OP cancellous bone. *Stud Health Technol Inf*. 2008;133:238—245.
14. Wang X, Yan Y, Pan Y, et al. Generation of three-dimensional hepatocyte/gelatin structures with rapid prototyping system. *Tissue Eng*. 2006;12:83—90.
15. Murphy SV, Atala A. 3D bioprinting of tissues and organs. *Nat Biotechnol*. 2014;32:773—785.